Detection of C8H- and Comparison with C8H toward IRC+10216

Remijan, A. J., Hollis, J. M., Lovas, F. J., Cordiner, M. A., Millar, TJ., Markwick-Kemper, A. J., & Jewell, P. R. (2007). Detection of C8H- and Comparison with C8H toward IRC+10216. *Astrophysical Journal*, *664*(1 II), L47-L50. https://doi.org/10.1086/520704

Published in:
Astrophysical Journal

The Astrophysical Journal, 664:L47–L50, 2007 July 20

DETECTION OF C_8H^- AND COMPARISON WITH C_8H TOWARD IRC +10 216

Anthony J. Remijan,[1] J. M. Hollis,[2] F. J. Lovas,[3] M. A. Cordiner,[4] T. J. Millar,[4]
A. J. Markwick-Kemper,[5] and P. R. Jewell[1]

Received 2007 May 16; accepted 2007 June 7; published 2007 June 27

ABSTRACT

We report the detection of new transitions of octatetraynyl (C_8H) toward the circumstellar envelope IRC +10 216 using data taken with the 100 m Green Bank Telescope (GBT). In addition, we report five features from the Ku, K, and Q bands that have been identified as transitions of the octatetraynyl anion (C_8H^-). From a rotational temperature diagram and an assumed source size of 30″, we find a total C_8H column density of $8(3) \times 10^{12}$ cm^{-2} and a rotational temperature of ~13 K. From the five detected transitions of C_8H^-, we find a total C_8H^- column density of $\sim 2.1 \times 10^{12}$ cm^{-2} consistent with a rotational temperature of ~34 K for a total C_8H/C_8H^- column density ratio of ~3.8. This observed C_8H/C_8H^- column density ratio is similar to the theoretical prediction of 3.6, while the observed column densities were lower than that predicted by a factor of ~30. This prompted us to reinvestigate the initial conditions of the circumstellar envelope (CSE) model. The new model results are presented, and they more closely match the C_8H and C_8H^- abundances observed with the GBT. Finally, we use the new CSE model results to predict the abundance of decapentaynyl ($C_{10}H$), and we compare them with the measured upper limit found from the GBT observations.

Subject headings: line: identification — radio lines: stars — stars: AGB and post-AGB — stars: individual (IRC +10 216)

Molecular anions have been important in astronomy for more than 70 years (e.g., Wildt 1939) and were predicted to be detectable in astronomical environments by Herbst (1981). Presently, molecular anions are predicted from chemical formation models to be in a high abundance, often comparable to their neutral counterparts, in various astronomical environments including dark clouds, the CSE of evolved stars, and photodissociation regions (see, e.g., Millar et al. 2000, 2007, and references therein). Recently, the laboratory detection of the hexatriynyl anion (C_6H^-) showed that several previously unidentified transitions present in the molecular line survey of Kawaguchi et al. (1995) toward IRC +10 216 were indeed due to the C_6H^- anion. The detection was further confirmed by observing two Ku-band transitions toward TMC-1 (McCarthy et al. 2006) with the GBT. Kasai et al. (2007) followed up on the initial 1995 survey results and detected two new transitions of C_6H^- at 7 and 3 mm wavelengths using the Nobeyama 45 m and IRAM 30 m radio telescopes. From a rotational temperature diagram and an assumed source size of 30″, they determined a total C_6H^- column density toward IRC +10 216 of $\sim 7 \times 10^{12}$ cm^{-2} and a rotational temperature of ~32 K. Furthermore, the relative abundance ratio between C_6H and C_6H^- was determined to be ~11.

Inspired by these recent detections of C_6H^-, and in order to test the formation models of large acetylenic chain radicals and their associated anions, we searched archival GBT data for additional, low-frequency transitions of octatetraynyl (C_8H) toward IRC +10 216 to follow up the initial detection by Cernicharo & Guélin (1996), and as such our search overlapped with several measured transitions in recent lab experiments by Gupta et al. (2007) of the associated octatetraynyl anion (C_8H^-). We also utilized the measured and predicted transitions by Gottlieb et al. (1998) to search for the next largest carbon chain radical, decapentaynyl ($C_{10}H$). In the work herein, we report the detection of new transitions of C_8H toward the CSE of IRC +10 216, including the first detection of C_8H transitions from the $^2\Pi_{1/2}$ state. In addition, we report five features from the Ku, K, and Q bands that have been identified as transitions of C_8H^-. Also, we reinvestigated the initial conditions of the CSE model of Millar et al. (2007) to more closely match the C_8H and C_8H^- abundances observed with the GBT. Finally, we use the new CSE model results to predict the abundance of $C_{10}H$, and we compare them with the measured upper limit found from the GBT observations.

Observations of the large carbon chains C_8H, $C_{10}H$, and C_8H^- were conducted with the NRAO[6] 100 m Robert C. Byrd GBT. The Ku- and K-band observations occurred between 2004 March 4–29 and 2005 April 1. The GBT spectrometer was configured in its eight intermediate-frequency (IF), 200 MHz, three-level mode, which is capable of observing four 200 MHz frequency bands at a time in two polarizations through the use of offset oscillators in the IF. This mode afforded a 24.4 kHz channel separation. The Q-band observations occurred in 2005 March–April, and the spectrometer was configured in its eight IF, 800 MHz, three-level mode, which is capable of observing four 800 MHz frequency bands at a time in two polarizations. This mode afforded a 390.7 kHz channel separation.

Antenna temperatures are on the T_A^* scale (Ulich & Haas 1976) with estimated 20% uncertainties. GBT half-power beamwidths can be approximated by $\theta_B = 740''/\nu$(GHz). The IRC +10 216 J2000 pointing position employed was $\alpha = 09^h50^m29.1^s$, $\delta = +12°29'27.9''$, and an LSR source velocity of -26.0 km s^{-1} was assumed. Data from the Ku- and K-band receivers were taken in the OFF-ON position-switching mode, with the OFF position 60′ east in azimuth with respect to the ON-source position. A single

[1] National Radio Astronomy Observatory, 520 Edgemont Road, Charlottesville, VA 22903-2475.
[2] NASA Goddard Space Flight Center, Computational and Information Sciences and Technology Office, Code 606, Greenbelt, MD 20771.
[3] Optical Technology Division, National Institute of Standards and Technology, Gaithersburg, MD 20899.
[4] Astrophysics Research Centre, School of Mathematics and Physics, Queen's University Belfast, Belfast BT7 1NN, UK.
[5] Jodrell Bank Centre for Astrophysics, School of Physics and Astronomy, University of Manchester, Sackville Street Building, Manchester M60 1QD, UK.

[6] The National Radio Astronomy Observatory is a facility of the National Science Foundation, operated under cooperative agreement by Associated Universities, Inc.

scan consisted of 2 minutes in the OFF-source position followed by 2 minutes in the ON-source position. Data from the Q-band receiver were taken in both the OFF-ON position-switching (PS) mode and the nod (beam-switching) mode. In the OFF-ON PS mode, the OFF position was 60′ east in azimuth with respect to the ON-source position. In the nod mode, the two beams of the GBT Q-band receiver are able to be switched by a separation of ∼1′. In both switching modes for the Q-band receiver, a single scan consisted of 5 minutes in the OFF-source position followed by 5 minutes in the ON-source position. The two polarization outputs from the spectrometer and the observations taken over multiple days were averaged in the final data reduction process to improve the signal-to-noise ratio.

Table 1 lists the rotational transitions of the molecules sought. The transition quantum numbers, the transition parity (if applicable), the calculated transition rest frequency, the energy of the upper level (K), the transition line strength multiplied by the square of the permanent dipole moment (D^2), and the telescope beam efficiency (η_B) are listed in the first six columns. In the seventh column, the fitted integrated line intensity and the associated 1 σ error (type A uncertainties with coverage factor $k = 1$; Taylor & Kuyatt 1994) at an LSR velocity of -26.0 km s^{-1} for IRC +10 216 are listed. In the case where no line was detected, a 1 σ noise limit of the intensity is given. The spectra for the C_8H and C_8H^- transitions toward IRC +10 216 are shown in Figures 1 and 2, respectively. In both Figures 1 and 2, the spectra are displayed on the same velocity scale, and each was Hanning-smoothed over 3 channels automatically during data processing. This holds in all cases except for Figure 1*d*, in which case, in order to show the detection of both the $^2\Pi_{1/2}$ and $^2\Pi_{3/2}$ transitions simultaneously, the passband range was extended. The identification of the other spectral features in the IRC +10 216 C_8H passbands were determined using the LOVAS/NIST Recommended Rest Frequencies Database (Lovas & Dragoset 2004), the JPL Molecular Spectroscopy Database (Pickett et al. 1998), and the Cologne Database for Molecular Spectroscopy (Müller et al. 2005). Unidentified transitions with their associated rest frequencies, assuming an LSR velocity of -26.0 km s^{-1}, were also labeled accordingly in each passband.

Since all the transitions of the large carbon chain toward IRC +10 216 were detected in emission, we assumed that all lines were optically thin and thus were able to estimate their total column densities from the usual radiative transfer emission expression (e.g., see eq. [1] of Remijan et al. 2005). The requisite molecular line parameters needed for evaluating N_T, the total column density expression, are given in Table 1 and associated footnotes. The total C_8H and C_8H^- column densities were determined using a rotational temperature diagram assuming a 30″ source size for the IRC +10 216 emitting region (Kasai et al. 2007). From the rotational temperature diagram of the $^2\Pi_{3/2}$ transitions of C_8H, we find a total C_8H column density of $8(3) \times 10^{12}$ cm^{-2} and a rotational temperature of $\sim 13 \pm 2$ K. In order to find the total column density for C_8H, the rotational partition function (Table 1, footnotes) is estimated for both Π states. From the five detected transitions of C_8H^-, we find a total C_8H^- column density of $1.5(6) \times 10^{12}$ cm^{-2} and a rotational temperature of $\sim 52^{+48}_{-18}$ K. The derived rotational temperature of 52 K for C_8H^- is higher than the values determined for other molecular anions toward IRC +10 216. For example, Kasai et al. (2007) accurately determined a rotational temperature of $\sim 32 \pm 2$ K for C_6H^-. Considering the large error bars on our C_8H^- rotational diagram, our data are consistent with a similar rotational temperature of ∼34 K that yields a total C_8H^- column density of 2.1×10^{12} cm^{-2} and, therefore, a total C_8H/C_8H^- column density ratio of ∼3.8.

TABLE 1
SUMMARY OF SPECTRAL LINE OBSERVATIONS TOWARD IRC +10 216

Transition	Parity	Frequency (MHz)	E_u (K)	$S_{ij}\mu^{2\,a}$	η_B	$\Delta T_A^* \, dv^b$ (mK km s^{-1})
Octatetraynyl (C_8H)[c]						
$^2\Pi_{3/2}$, $J = 23/2–21/2$	e/f	13493.392	3.95	1904.9	0.92	141(33)
$^2\Pi_{3/2}$, $J = 31/2–29/2$	e/f	18186.717	7.10	2588.6	0.89	202(60)
$^2\Pi_{3/2}$, $J = 39/2–37/2$	e/f	22880.019	11.16	3274.2	0.85	290(74)
$^2\Pi_{3/2}$, $J = 73/2–71/2$	e/f	42826.131	38.48	6157.6	0.60	205(75)
$^2\Pi_{3/2}$, $J = 75/2–73/2$	e/f	43999.405	40.59	6326.9	0.58	198(78)
$^2\Pi_{3/2}$, $J = 77/2–75/2$	e/f	45172.674	42.76	6496.1	0.56	86(26)
$^2\Pi_{1/2}$, $J = 73/2–71/2$	e	42907.773	66.47	3083.1	0.60	325(61)
$^2\Pi_{1/2}$, $J = 73/2–71/2$	f	42917.314	66.48	3083.3	0.60	265(93)
Decapentaynyl ($C_{10}H$)[d]						
$^2\Pi_{3/2}$, $J = 49/2–47/2$	e/f	14761.625(2)	9.00	2742.8	0.91	<1.5 mK[e]
$^2\Pi_{3/2}$, $J = 73/2–71/2$	e/f	21991.718(11)	19.76	4099.2	0.86	<2.5 mK[e]
Octatetraynyl anion (C_8H^-)[f]						
$J = 22–21$		25666.783(3)	14.18	3115.4	0.82	119(36)
$J = 35–34$		40833.075(18)	35.32	4956.4	0.63	282(84)
$J = 36–35$		41999.690(20)	37.33	5098.0	0.61	276(92)
$J = 37–36$		43166.302(22)	39.41	5239.6	0.59	206(60)
$J = 38–37$		44332.910(24)	41.54	5381.2	0.57	186(66)

[a] The transition line strengths are taken from Müller et al. (2005).
[b] The error shown in the integrated line intensity is 1 σ (type A coverage $k = 1$; Taylor & Kuyatt 1994).
[c] The listed rest frequencies taken from McCarthy et al. (1999) were averaged over both parity states and are good to 10–20 kHz; $\mu_a = 6.5$ D, and $Q_{rot} = 2125$ at 13 K.
[d] The rest frequencies are taken from Gottlieb et al. (1998); $\mu_a \sim 7.5$ D, and $Q_{rot} = 3367$ at 13 K.
[e] No spectral feature detected (1 σ rms noise level listed).
[f] The rest frequencies are taken from Gupta et al. (2007); $\mu_a \sim 11.9$ D, and $Q_{rot} = 1215$ at 34 K.

Given the column density measurements of the GBT observations, it is clear that the current formation model of Millar et al. (2007) overestimates the measured column densities of C_8H and C_8H^-. Yet the measured abundance ratio of ∼3.8 is close to the predicted value of 3.6. Thus, in order to account for the measured column density of C_8H and C_8H^-, we reinvestigated the initial conditions of the Millar et al. (2007) model and ran the calculation for new values of the initial fractional abundance of acetylene (C_2H_2) with respect to molecular hydrogen (H_2). Table 2 lists the new column density predictions of the large acetylenic chain radicals and their associated anions of the IRC +10 216 chemical model calculated for new values of the fractional abundance of C_2H_2. This is because the formation of C_8H, and the other large C chains, is largely dependent on the initial C_2H_2 abundance since C-chain growth is dominated by the addition of C_2 units. For example, the formation of C_8H and C_8H^- begins with $C_2H + C_6H_2 \rightarrow C_8H_2 + H$, and then associated dissociative reactions form C_8H and C_8H^-: $C_8H_2 + h\nu \rightarrow C_8H + H$ and $C_8H + e \rightarrow C_8H^- + h\nu$.

Figure 3 shows the model results for C_8H, C_8H^-, $C_{10}H$, and $C_{10}H^-$ versus the CSE radius (cm). From the model results presented in Table 2, we find a peak C_8H column density of 2.5×10^{12} cm^{-2} and a peak C_8H^- column density of 6.1×10^{12} cm^{-2} for an initial C_2H_2 fractional abundance of $\sim 1 \times 10^{-5}$ with respect to H_2. In both cases, the new model predictions of C_8H and C_8H^- are within a factor of 3 of the measured values of our GBT results. Furthermore, comparing the new results with the measured column densities of C_6H and C_6H^-, the new model predictions are within a factor of 6 and 4, respectively. Thus, the new model predicts an abundance of both C_8H and C_8H^-

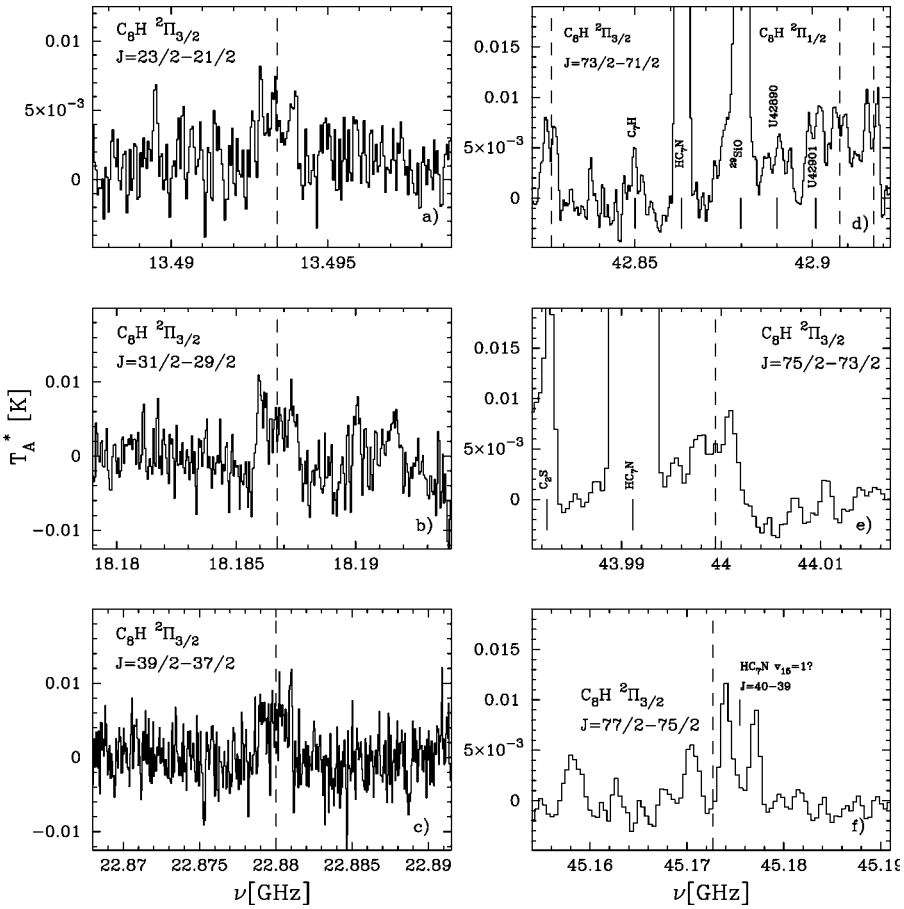

FIG. 1.—Octatetraynyl (C_8H) spectra toward IRC +10 216. Transition quantum numbers are shown in each panel. Spectra are displayed on the same velocity scale, except for panel *d* (see text), and were Hanning-smoothed over 3 channels automatically during data processing. The rest frequency of the listed transition is shown by the dashed line. All transitions and unidentified line rest frequencies were labeled assuming an LSR velocity of −26.0 km s^{-1}.

much closer to the measured values of our GBT results and to the published C_6H and C_6H^- results of Kasai et al. (2007).

However, there is still a clear discrepancy between the model results and the observed abundances. In the cases of C_6H and C_8H, the model results underestimate the observed abundances, and likewise in the cases of C_6H^- and C_8H^-, the model results overestimate the abundances. However, it is clear that by adjusting the initial C_2H_2 fractional abundance, we obtain a better fit to the observational results. All currently published formation models overestimate the abundance of both the radical and the anion by a factor of ~30. In addition, the cyanopolyyne HC_3N is also overestimated in current formation models (Millar et al. 2000), and this clearly suggests that the initial hydrocarbon fractional abundances are too high. Finally, the primary reason why even our current model cannot predict the measured abundance of the radicals and anions is most likely due to a lack of knowledge about the formation and destruction of these species. When more reaction rates are measured or better reaction rates are calculated, column density predictions closer to the observed values will most likely be attained.

The chemical model also predicts a peak $C_{10}H$ column density of 5.0×10^{11} cm^{-2}. Assuming that C_8H and $C_{10}H$ are cospatial, we obtain a 1 σ upper limit of $N_T < 1 \times 10^{12}$ cm^{-2}, which is above the predicted column density, for the $^2\Pi_{3/2}$, $J = 49/2–47/2$ *e*/*f* transition at 14761.6 MHz assuming an average line width of 29 km s^{-1}. Given the column density predicted from the model, the expected line intensity for this transition should be ~0.1 mK. Assuming good weather conditions at the GBT ($T_{sys} = 20$ K), achieving an rms value of ~0.03 mK in order to detect this transition at greater than the 3 σ level would require >1000 hr. Thus, unless the column density of $C_{10}H$ predicted by our model is too low by several orders of magnitude, the detection of $C_{10}H$ in the CSE of IRC +10 216 will need to wait for further advances in instrumentation.

Finally, the model predicts that the peak abundances of C_8H, C_8H^-, $C_{10}H$, and $C_{10}H^-$ occur at slightly different radii in the CSE (Fig. 3), although we note that the fractional abundance is not necessarily a good proxy for emission since species with high dipole moments will be excited only at high densities. From the rotational temperature diagram calculations, we infer that the distribution of C_8H is more extended in the CSE because of the low rotational temperature (~13 K), whereas the distribution of the C_8H^- anion is more compact because of the higher measured rotational temperature (~35–50 K). However, the chemical model clearly shows that the peak of both C_8H and C_8H^- occur at nearly the same radii. Thus, to obtain a more accurate representation of the column density and distribution of these large C-chain species, high-resolution interferometer observations of the CSE of both neutrals and anions are necessary.

In summary, we detected new low-frequency transitions of C_8H using archival GBT data toward IRC +10 216, including the first detection of C_8H transitions from the $^2\Pi_{1/2}$ state to follow up the initial detection by Cernicharo & Guélin (1996). In addition, we reported five transitions from the Ku, K, and Q bands that have been identified as transitions of C_8H^-. By reinvestigating the initial conditions of the CSE model of Millar et al. (2007), we were effective in matching the measured column densities of C_8H and C_8H^- to the model predictions and,

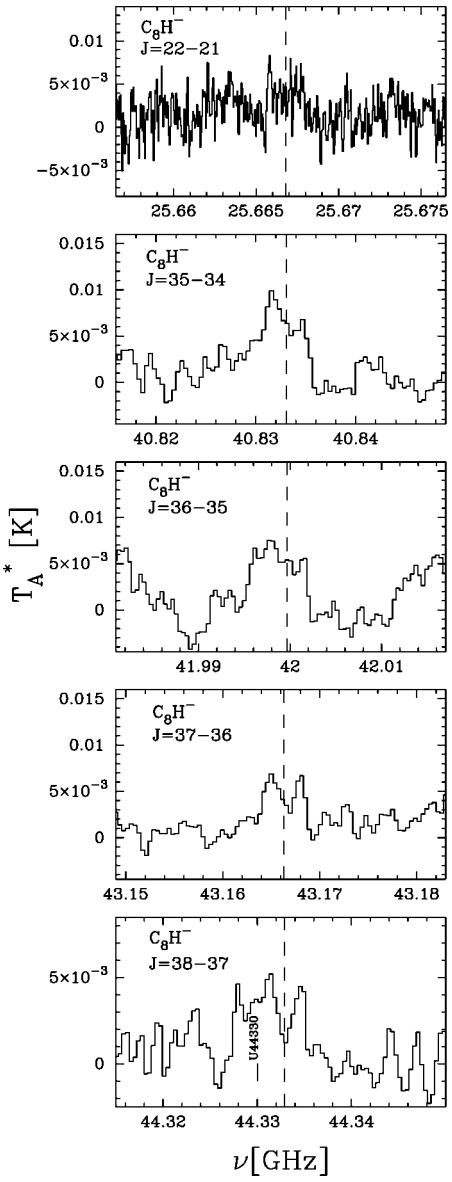

FIG. 2.—Octatetraynyl anion (C_8H^-) spectra toward IRC +10 216. Transition quantum numbers are shown in each panel. The rest frequency (Table 1), assuming an LSR velocity of −26.0 km s^{-1} of the displayed transition, is shown by the dashed line.

TABLE 2

PREDICTED COLUMN DENSITIES AS A FUNCTION OF C_2H_2 FRACTIONAL ABUNDANCE

SPECIES	$X(C_2H_2)$ 5×10^{-5}	1×10^{-5}	4×10^{-6}
C_4H	1.3×10^{15}	1.7×10^{14}	3.7×10^{13}
C_4H^-	1.0×10^{13}	6.4×10^{12}	2.2×10^{12}
C_6H	5.7×10^{14}	1.3×10^{13}	1.2×10^{12}
C_6H^-	1.7×10^{14}	2.7×10^{13}	3.9×10^{12}
C_8H	2.1×10^{14}	2.5×10^{12}	2.0×10^{11}
C_8H^-	5.8×10^{13}	6.1×10^{12}	7.1×10^{11}
$C_{10}H$	5.8×10^{13}	5.0×10^{11}	3.2×10^{10}
$C_{10}H^-$	2.3×10^{13}	1.5×10^{12}	1.2×10^{11}

NOTE.—The column densities (in units of cm^{-2}) and fractional abundances (Fig. 3) for the radicals include both $^2\Pi_{1/2}$ and $^2\Pi_{3/2}$ states.

as such, the column density ratio between the neutral and anion. We also predicted the $C_{10}H$ column density and showed that the detection of $C_{10}H$ in IRC +10 216 will need to wait for the next generation of instrumentation. Finally, in order to further investigate the distribution of large C-chain species in the CSE of IRC +10 216 to compare with the formation models, high-resolution interferometer observations of both radicals and anions are necessary.

Astrophysics at QUB is supported by a grant from the STFC. M. A. C. thanks QUB for support. Finally, we thank an anonymous referee for a favorable review and valuable comments on this work

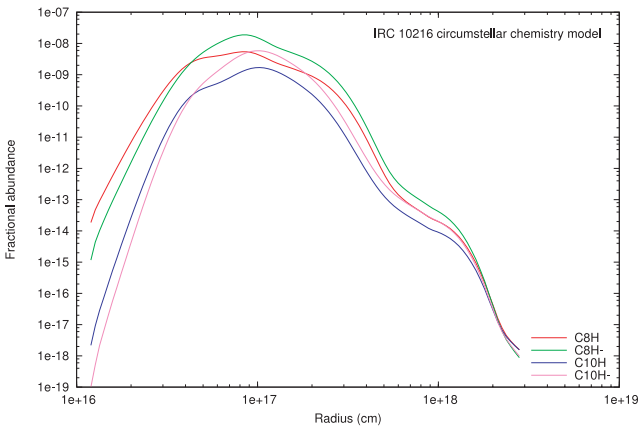

FIG. 3.—IRC +10 216 chemical model results for C_8H, C_8H^-, $C_{10}H$, and $C_{10}H^-$ abundances (relative to the the total number density of H_2) vs. the radius (cm).

REFERENCES

Cernicharo, J., & Guélin, M. 1996, A&A, 309, L27
Gottlieb, C. A., McCarthy, M. C., Tavers, M. J., Grabow, J.-U., & Thaddeus, P. 1998, J. Chem. Phys, 109, 5433
Gupta, H., Brünken, S., Tamassia, F., Gottlieb, C. A., McCarthy, M. C., & Thaddeus, P. 2007, ApJ, 655, L57
Herbst, E. 1981, Nature, 289, 656
Kasai, Y., Kagi, E., & Kawaguchi, K. 2007, ApJ, 661, L61
Kawaguchi, K., Kasai, Y., Ishikawa, S.-I., & Kaifu, N. 1995, PASJ, 47, 853
Lovas, F. J., & Dragoset, R. A. 2004, NIST Recommended Rest Frequencies for Observed Interstellar Molecular Microwave Transitions—2002 Revision (Ver. 2.0.1), http://physics.nist.gov/restfreq
McCarthy, M. C., Chen, W., Apponi, A. J.,Gottlieb, C. A., & Thaddeus, P. 1999, ApJ, 520, 158
McCarthy, M. C., Gottlieb, C. A., Gupta, H., & Thaddeus, P. 2006, ApJ, 652, L141
Millar, T. J., Herbst, E., & Bettens, R.P.A. 2000, MNRAS, 316, 195
Millar, T. J., Walsh, C., Cordiner, M. A., Ní Chuimín, R., & Herbst, E. 2007, ApJ, 662, L87
Müller, H. S. P., Schlöder, F., Stutzki, J., & Winnewisser, G. 2005, J. Mol. Struct., 742, 215
Pickett, H. M., Poynter, R. L., Cohen, E. A., Delitsky, M. L., Pearson, J. C., & Müller, H. S. P. 1998, J. Quant. Spectrosc. Radiat. Transfer, 60, 883
Remijan, A. J., Hollis, J. M., Lovas, F. J., Plusquellic, D. F., & Jewell, P. R. 2005, ApJ, 632, 333
Taylor, B. N., & Kuyatt, C. E. 1994, NIST Tech. Note 1297 (Washington, DC: US GPO)
Ulich, B. L., & Haas, R. W. 1976, ApJS, 30, 247
Wildt, R. 1939, ApJ, 89, 295